LAWRENCE
LIVERMORE
NATIONAL
LABORATORY

UCRL-JRNL-204455

Inertial Confinement Fusion Materials Science

Alex V Hamza

June 2, 2004

Encyclopedia of Materials: Science and Technology

Inertial Confinement Fusion Material Science

Alex V. Hamza
Nanoscale Synthesis and Characterization Laboratory
University of California, Lawrence Livermore National Laboratory

1.0 Introduction

Demonstration of thermonuclear ignition and gain on a laboratory scale is one of science's grand challenges. The National Ignition Facility (NIF) is committed to achieving inertial confinement fusion (ICF) by 2010. Success in this endeavor depends on four elements: the laser driver performance, target design, experimental diagnostics performance, and target fabrication and target materials performance. This article discusses the current state of target fabrication and target materials performance. The first three elements will only be discussed insofar as they relate to target fabrication specifications and target materials performance. Excellent reviews of the physics of ICF are given by Lindl [Lindl 1998] and Lindl *et al.* [Lindl 2004].

To achieve conditions under which inertial confinement is sufficient to achieve thermonuclear burn, an imploded fuel capsule is compressed to conditions of high density and temperature. In the laboratory a driver is required to impart energy to the capsule to effect an implosion. There are three drivers currently being considered for ICF in the laboratory: high-powered lasers, accelerated heavy ions, and x rays resulting from pulsed power machines. Of these, high-powered lasers are the most developed, provide the most symmetric drive, and provide the most energy.

Laser drive operates in two configurations. The first is direct drive where the laser energy impinges directly on the ICF capsule and drives the implosion. The second is indirect drive, where the energy from the laser is first absorbed in a high-Z enclosure or hohlraum surrounding the capsule, and the resulting x-rays emitted by the hohlraum material drives the implosion.

Using direct drive the laser beam energy is absorbed by the electrons in the outer corona of the target. The electrons transport the energy to the denser shell region to provide the ablation and the resulting implosion. Laser direct drive is generally less efficient and more hydrodynamically unstable than the x-ray driven ablation of indirect drive. The symmetry of the implosion depends sensitively on the balance of the intensity of the individual beams driving the target. Variations in intensity imprint perturbations on the target that are amplified by hydrodynamic instabilities.

Indirect drive is less efficient at coupling energy to a capsule than direct drive because of the conversion to x-rays in the hohlraum. However, indirect drive is less sensitive to variations in beam intensity and hydrodynamic instabilities. The ignition threshold for directly-driven and indirectly-driven targets is about the same. However, the gain is calculated to be about a factor of 2 greater in directly driven targets.

Accelerated heavy ion driven ICF is also an indirect-drive method. The heavy ions impinge on a radiation converter that generates x-rays in a hohlraum. The physics of heavy ion driven ICF is, thus, much the same as for indirect drive.

Z-pinch driven x-ray sources, such as the Z machine [Mehlhorn 2003] at Sandia National Laboratories also can drive ICF capsules. Again, since the x-rays generated drive the capsule, the physics is much the same as indirect laser driven capsules.

In order to achieve conditions for ICF, targets have a spherical shell filled with a low density ($\leq$ 1 mg/cm^3) equimolar mixture of deuterium and tritium (DT) gas. The spherical shell consists of an outer ablator and an inner region of frozen or liquid DT. Energy from the driver is delivered to the ablator which heats up and expands. As the ablator expands the rest of the shell is forced inward to conserve momentum. The capsule behaves as a spherical, ablation-driven rocket. As the capsule implodes, PdV work heats a central region. Electron conduction and radiative losses act to cool the central region. Fuel convergence ratios of 30-40 and a central fuel temperature of 10 keV are required so that α particle deposition from thermonuclear burn of DT can overcome conduction and radiative losses and a self-sustaining burn wave can be generated. An asymmetric implosion will convert less of the available energy into compression. Assuming the available energy is such that a 25% variation in symmetry is tolerable at peak fuel compression, then less than 1% variation in symmetry is acceptable in the pre-compressed capsule.

Hydrodynamic instabilities, such as the classical Rayleigh-Taylor fluid instability, set the upper limit of the shell compression. Hydrodynamic instabilities set the achievable implosion velocity, which in turn defines the energy required for ignition. In addition during compression the hydrodynamic instabilities cause mixing of the cold fuel with the central, hot region. A widely used formula for the growth of Rayleigh-Taylor perturbations is given by [Lindl 1983]:

$$\gamma = \sqrt{\frac{At \times k \times a}{1 + At \times k \times L}} - \beta \times k \times v_a \qquad \text{(eq.1)}$$

Where γ is the growth rate, At is the Atwood number, k is the mode wave number of the perturbation, a is the acceleration, L is the density gradient scale length in the ablation front, β is a constant between 1 and 3, and v_a is the ablation velocity. The Atwood number is the dimensionless density difference between the two interacting fluids, $At = (\rho_1-\rho_2)/(\rho_1+\rho_2)$. In indirect-drive experiments β is ~1 and in direct-drive experiments β is ~3. However, since the ablation velocity is ~ a factor-of-10 higher for indirect drive versus direct drive, the Rayleigh-Taylor growth rate is lower for indirect-drive experiments. The growth factors are typically between 200 and 1000. So, for a 100 μm thick ablator, perturbations on the surfaces must be less than 100 nm. As discussed below, since there are more than one interface the initial perturbation must be significantly less than 100nm in practice.

2.0 Target Design

The NIF baseline target design is a spherical cryogenic capsule consisting of DT gas, solid DT shell and a low-Z ablator shell (see figure 1.). The cryogenic capsule is enclosed in a cylindrical high-Z hohlraum with two laser entrance holes at each end (see figure 2).

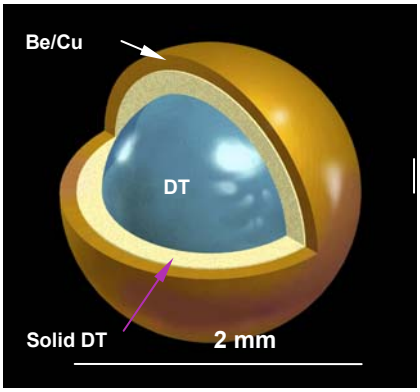

Figure 1. Schematic of Cryogenic ICF target

Three possible ablators are currently under evaluation: Br-doped CH, Cu-doped Be and polyimide ablators. CH is a carbon hydrogen polymer CH_n with n~1.3. The dopants, Br and Cu, are added for x-ray "preheat" control. The high energy tail of the x-rays generated by the laser drive impinging on the hohlraum walls can penetrate the ablator and "preheat" the fuel. The higher Z dopants can absorb these x-rays. However, varying the dopant concentration radially in the ablator has the potential benefit of increasing the length scale over which the density gradient changes to retard instability growth (denominator in equation 1).

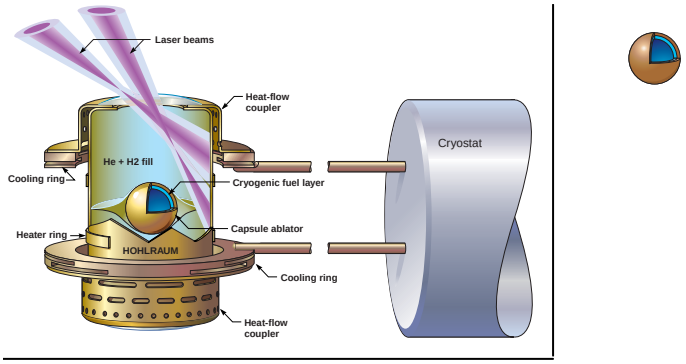

Figure 2. Baseline ICF target inside a cryogenic hohlraum

As mentioned above, the capsules, and hence ablators, must be symmetrically fabricated. A 25% deviation from spherical at peak implosion might be tolerable with sufficient energy absorbed by the capsule to still reach ignition. A 25% deviation at peak implosion (convergence of 30-40) corresponds to a 1% deviation from spherical as fabricated.

Radiation-hydrodynamic simulations of instability growth on all three ablator designs have been performed. While all interfaces contribute to the performance of the capsule, perturbations on the outer surface of the ablator and the inner surface of the DT ice are expected to most sensitively affect the performance. These calculations predict that CH + Br ablator performance will be adequate with a surface root mean square (rms) roughness of 15 nm or less with a smooth DT ice layer (less than 0.5 micron rms roughness). The polyimide and Be+Cu ablator will perform adequately with surface rms roughness of 50 nm or less with a smooth DT ice layer (less than 1 micron rms roughness). Be has a lower albedo (albedo is the fraction of light reflected by a body) than CH and, thus, Be absorbs energy more efficiently leading to higher ablation velocities and hence lower instability growth rates. Because of the low-Z of these ablators, the hot coronas do not absorb energy very well, which improves the efficiency of the ablation.

The implosion is very sensitive to non-uniformities in the density and opacity of the ablator. As an estimate of the sensitivity a 30 nm roughness on the surface for a ~150 micron thick ablator corresponds to a 1 in 5000 variation in areal density. In addition the implosion is very sensitive to shock timing during the drive. The fuel entropy should be kept as low as possible to allow for the highest compressibility. Keeping the fuel entropy sufficiently low requires careful timing of four successive shocks to bring the fuel to optimal compression. The timing of the first shock depends on its propagation through the ablator. The sound speed is known to depend on the crystal orientation in beryllium. Thus, the grain structure of the beryllium may perturb the first shock. A non-uniform columnar grain structure may adversely affect performance.

All the single-shell ignition targets require that the bulk of the fuel reside in a cryogenic layer on the inside surface of the ablator. For smooth ablators (<15 nm rms) simulations predict adequate performance for a CH ablator with the DT ice roughness less than 0.5 micron rms, a polyimide ablator with the DT ice roughness less than 1 micron rms, and a beryllium ablator with the DT ice roughness less than 2 micron rms.

Bulk heating of the DT by β decay of the tritium provides a technique to produce smooth DT ice layers. If the ablator is held at a uniform temperature, β decay will cause thick regions to be at a higher temperature than thinner regions. Sublimation of DT from the hotter regions will produce a DT ice layer of nominally uniform thickness. DT deposits usually as small crystallites. β layering does not eliminate discontinuities at the boundaries of crystallites, resulting in about 1 micron rms roughness at the triple point of DT.

β layering can be improved upon by external heating. Optical heating that couples to rovibrational transitions in DT and radio-frequency heating that couples to free electrons produced by β decay have been shown to produce smoother DT layers [Collins]. The optical technique requires transparent ablator shells and the radio-frequency technique requires non-conducting ablator shells. Unfortunately, Be ablators are both opaque in the visible and conducting.

Low-density foam could be used as a matrix for the cryogenic fuel layer. A foam-filled fuel layer has a higher ignition temperature, which depends on foam density and material composition. Important properties of such DT wicking in nearly porous materials is not known. In particular, since pore or cell sizes must be below 1 micron in order not to seed hydrodynamic instabilities, no data on DT wicking and wetting are available for nanoporous materials.

The double shell ICF design is an alternative to the single shell cryogenic design. Figure 3 shows double shell target. The original design advantage of the double shell depended on velocity multiplication. During implosion the massive outer shell collides with the much lighter inner shell and accelerates it to a higher velocity. In the limiting case where the inner shell mass is negligible compared to the mass of the outer shell and the collision is elastic, the inner shell can reach twice the velocity of the outer shell. Recent simulations have shown however, that there is not a significant velocity multiplication when the shells collide. There are other advantages that still make the double shell design interesting. Since volume ignition, used in the double shell design, requires a lower velocity than "hot spot" ignition in a single shell design, the double shell design may ignite at lower absorbed energy than a single shell design [Amendt 2002]. The inner shell must be high Z for efficient high density compression of the fuel contained within it. The high density of the inner shell makes it able to with stand a high pressure shock and still compress the fuel. The high density shell inertially confines the fuel for longer time creating a more efficient burn. Also, because the inner shell is high Z, the shell contains the radiation emission from the fuel as it compresses and further lowers the ignition threshold. However, the potential advantages of inertial and radiation containment ignore the effects of hydrodynamic instability during the collision of the two shells. The massive, low-density outer shell is pushing on a lighter, high-density inner shell. This is a classically Rayleigh-Taylor unstable situation. Without stringent control of this interface during collision the design entails significant risk. In addition the smaller amount of fuel contained in the non-cryogenic double shell design make it a lower gain target.

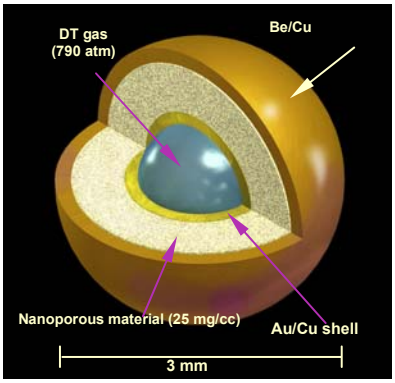

Figure 3. Schematic of Double shell ICF target

The inner shell has stringent requirements. In order to keep its mass small compared to the outer shell it must be a thin shell. The thin inner shell must be sufficiently strong to contain ~1000 atmospheres of fuel. For these dimensions (~ 650 micron diameter and

~50 micron thickness) a tungsten shell has been demonstrated by Los Alamos National Laboratory to have the requisite strength (~700 MPa) [Varnum]. As mentioned above, the inner shell must be high Z to contain the radiative emission and have high density to with stand the high pressure shock during the collision of the shells. Recent designs of double shell targets have concentrated on control of the hydrodynamic instability that occurs during the collision of the shell. In the double shell the design cannot take advantage of ablative stabilization (the negative term in equation 1). However, the double shell design can take advantage of an increase in the length scale over which the density gradient occurs during the collision (the denominator in equation 1). This requires producing an inner shell with a density gradient from high density to a lower density at the outer surface of the inner shell. The current design calls for an inner shell with pure Au at the inner surface of the inner shell and grading the density by alloying the Au with increasing amounts of Cu until the outer surface of the inner shell is pure Cu.

In order for the double shell ICF target to perform adequately the two shells must be concentric to with in 3-5 microns [Amendt 2002]. In order to minimally impede the outer shell collision with the inner shell, there should be as little density as possible between the shells. The material between the shells must be uniform on the length scales that can seed instabilities (~1 to 100 microns). The double shell design calls for an ultralow density (25-50 mg/cm^3) material with sub 500 nm pore sizes with composition to match the outer surface of the inner shell (Cu) and to support the inner shell concentrically within the outer shell. Recently performed experiments on the OMEGA laser at the University of Rochester with double-shell targets measured neutrons from the DD reaction demonstrating efficient compression of the D_2 gas [Amendt 2004]. The target materials in this experiment were a Ge-doped CH outer shell, a CH inner shell containing 50 atmospheres of D_2 gas, and a carbonized resorcinol foam with 50 mg/cm^3 density and sub 100nm pores. Double-shell capsules with poorly joined outer-shell hemispheres, ultralow density material with greater than 1 micron pore sizes, or stalks or tents to position the inner shells have not demonstrated compression.

Hohlraums for indirect drive experiments are generally cylindrical with laser entrance holes on each side. Gold hohlraums are made in a three step process. First a mandrel (Cu) is machined to shape, usually by single point diamond turning. The mandrel is coated by electroplating with gold and the mandrel is finally etched away.

The opacity and albedo properties of the hohlraum material are critical to its performance. Any single material will have holes (lower opacity regions) in the photon energy region of interest. Thus, cocktail hohlraums have been proposed which use a combination of materials to fill opacity holes and reduce wall energy losses. For example, calculations show Gd opacity complements Au opacity in the 0.1 to 10 keV photon energy range [Orzechowski 1996]. The Au/Gd hohlraum can increase indirect-drive efficiency by reducing the wall losses of the hohlraum by 15%.

Hohlraum efficiency can also be improved by reducing wall motion during the radiation of energy in the hohlraum. Energy that goes into ablating material from the hohlraum wall is energy that is not absorbed by the capsule. One way to reduce the fraction of

energy that goes into the wall motion is to reduce the density of the holhraum wall, but maintain the atomic number. Thus, a high-Z low density foam liner could improve the hohlraum coupling efficiency to the capsule. Simulations have shown that a porous gold liner with density of 200 – 500 mg/cm^3 could improve the hohlraum coupling by ~15% [Rosen 2004]. At 1.8 MJ of laser energy (NIF) a 15% reduction in wall losses corresponds to nearly 100 kJ in energy savings.

3.0 Target Materials

Target materials for ICF consist of two types: materials for shells and nanocellular materials. Microshells are the staple of targets for ICF. Today most capsules are polymer or glass microshells.

Many of the capsules produced for laser driven ICF experiments are made using a depolymerizable mandrel. The poly (α-methyl-styrene) PAMS mandrel is produced by micro-encapsulation. The immiscibility of oil and water is used to produce liquid shells of polymer material dissolved in the hydrophobic solvent. Upon proper curing and drying, solid polymer shells are formed. Surface tension forces the shells to have excellent symmetry and the immiscibility creates shells with good wall uniformity (<5%) with diameters from 200 microns to 5 mm. A wall uniformity of 1% is required (see section 2 above). Since many shells are easily produced the best shells can be selected for experiments. Wall thicknesses are typically limited to 10-20% of the diameter size and wall thickness uniformity becomes worse as the wall thickness is increased.

Glow discharge polymer (GDP) or plasma polymer shells are produced by overcoating PAMS shells and then decomposing the PAMS mandrel. Depending on the plasma conditions and process gas(es) used the GDP coating can be composed of various doped CH based materials. The materials can be deposited in various combinations to produce shells containing several different layers. Glass capsules can be made by two techniques. The first technique involves a silicon-doped glow discharge polymer coating [Hoppe 2002]. The silicon-doped plasma polymer is subsequently oxidized in air, converting the silicon into SiO_2 and removing carbon and hydrogen by their conversion to CO_2 and water. These capsules have good wall uniformity (<5%) and less than 10 nm rms roughness. The second technique utilizes a heated drop tower.

Polyimide ablators perform intermediate to CH and Be ablators in design simulations, but since they are transparent in the optical, rovibrational smoothing can be used with polyimide ablators. An evaporative coating technique for thick polyimide ablator layers has been developed [Letts 2004]. The polyimide coating technique uses stoichiometriclly controlled fluxes from two Knudsen sources containing dianhydride and a diamine to deposit polyamic acid coatings. Heating the polyamic acid coating to 300º C converts the coating to polyimide. Coated shells are rough due to particles and damage caused by agitation to ensure a uniform coating. A smoothing process that exposes the initially rough polyamic acid coating to solvent vapor using levitation has been developed. Vapor smoothed coating of polyimide 160 microns thick with 20 nm rms surface roughness have been produced.

At Los Alamos National Laboratory, the Be capsule development is focused on precision machining of Be/Cu alloy hemishells and subsequent bonding of the hemishells under high pressure DT gas [Nobile 2004]. At Lawrence Livermore National Laboratory, Be/Cu capsules are being developed using sputter deposition of Be and Cu onto polymer mandrels [Jankowski 2002]. It is desirable to produce homogeneous, isotropic, dense, and mechanically strong Be coatings. One way to develop these properties is to refine the grain size to the nanoscale. The compositional effects of Cu, Fe, and B additions on the microstructure have been studied. Fe and B are found to have a dominant effect on grain refinement, capable of producing sub 20 nm grains. Research is also underway to develop DT filling methods for sputter deposited capsules by laser drilling a small hole (3-5 microns) followed by laser sealing.

Be 0.9 At. % Cu alloy has been synthesized by blending beryllium powder (<75 micron particles) and copper flakes (submicron particles) and hot isostatically pressing for 4 hours at 1000º C at 103 MPa [Nobile 2004]. Equiaxed 10-50 micron grains were produced. Higher atomic number impurity at the grain boundaries is likely oxide, common in powder synthesis techniques. A second technique is arc-melting Be/Cu to eliminate oxide impurities. The as cast Be/Cu is subsequently extruded by equal channel angular extrusion and annealed to refine grain size. Equiaxed 20 micron grains have been produced [Alexander 2004].

Producing smooth thin capsules with sufficient strength to contain ~1000 atms requires novel materials research. The Hall-Petch effect of refining grain-size of metals to increase strength is well known. To achieve the strength required this effect will need to be pushed to its limits. For example a coarse grain Au/Cu alloy (to be used in double shell ignition designs) has a yield strength of 60 MPa; for use as capsule material a yield strength of 450 MPa is required. To produce this increase in strength, grain size between 10-20 nm will be required. At this grain size the empirical Hall-Petch relation breaks down. It is in this regime of grain size where the transition from standard plasticity to new deformation mechanisms occurs. There is significant controversy in the literature over the transition and the new controlling deformation mechanism [Wolf 2004, van Swygenhoven 2003]. Presently the required increase in strength at the nanometer scale has been demonstrated only for face-centered-cubic nickel and copper [van Swygenhoven 2004]. In addition, grain refining also helps the capsules meet the smoothness requirements so as not to seed instabilities during the implosion.

Since materials with cell or pore sizes greater than 1 micron can seed instabilities only materials with sub-micron cell or pore sizes are discussed.

A recent review has discussed the chemistry and application of aerogels [Pierre 2002]. Only specific application to ICF will be discussed here. Aerogel preparation will be discussed only briefly.

Resorcinol formaldehyde aerogel is produced by reacting resorcinol and formaldehyde. The resulting polymer gel (sol-gel) is supercritically dried with CO_2 to produce an aerogel

with density in the 20-850 mg/cm^3 range [Pekala 1989]. The resorcinol-formaldehyde aerogel can be molded and used or it can be heated to 1000º C in an inert atmosphere where it becomes an almost pure carbon foam with pore size sub 100 nm. Hibbard et al. [Hibbard 2004] have used carbonized resorcinol-formaldehyde foam in their double-shell ICF target construction.

Silica aerogels were the first aerogel produced; they were developed for Cherenkov radiation detectors in the 1970's [Boudinaud 1976]. They also have sub 100nm pore size and can be produced in monolithic form at densities from 700 to 1 mg/cm^3 (the density of air). Silica aerogels can be machined or molded to shape in most cases. Doped silica aerogels have found application as backlighter materials for in situ x-ray radiography of laser targets (see below). Silica aerogels have also been used as catchers to recover shrapnel from laser irradiated targets.

Metal nanoporous materials with sub micron pore or cell sizes have only been reported since the 1990's. There are two main techniques for their production: dealloying and templating. They have not yet been employed in ICF targets because materials with suitable density and pore size and mechanically stability have not yet been produced.

Many nanoporous metals have been synthesized by dealloying [Pugh 2003]. In the dealloying technique, a homogeneous binary mixture of relatively noble metals is etched in, usually, nitric acid solution under an applied potential. The less noble metal is etched completely away over time and a nanoporous more noble metal material remains. The morphology of a typical dealloyed structure is a highly tortuous, completely interconnected porosity with a pore diameter as small as 3 nm. The structures can be coarsened to larger length scales by annealing at elevated temperatures [Sieradzki 1992]. Dealloying would be limited to the surface unless a mechanism exists for penetration throughout the alloy. Recently Erlebacher and Sieradzki and Erlebacher et al. [Erlebacher 2003, Erlebacher 2001] have discussed the mechanism for porosity to "grow" into the bulk via surface diffusion and capillary action. Figure 4 shows the results of the dealloying process for dealloying of a $Au_{0.3}Ag_{0.7}$ alloy producing nanoporous Au.

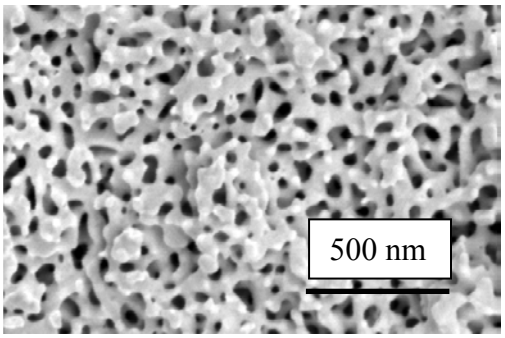

Figure 4. Scanning electron microscope image of nanoporous Au at 30% full density formed by dealloying $Au_{0.3}Ag_{0.7}$. The 500nm fiducial is shown. Image courtesy of Luke Hsuing (LLNL).

Close-packed colloidal crystals are promising precursors for novel materials. Velev et al. [Velev 1999] have demonstrated the formation of nanoporous Au via colloidal templating. A close-packed crystal of latex spheres was carefully infiltrated with Au nanoparticles in solution. After drying, the Au nanoparticles were sintered and the latex spheres decomposed, leaving behind a nanoporous Au with ~700 nm cell size and low density. Au nanoporous flakes of ~800 microns in diameter and a few microns thick were produced. Because of the sintering of Au nanoparticles was used to form the backbone, the density (not characterized) may have been quite low. The size of the sample needs to be increased and the mechanical properties determined to make a useful material for ICF applications, such as hohlraum liners. Figure 5 shows the results of the templating process for producing porous Cu/Ti. The template was produced from 6 micron carbon spheres. The interstial space was infiltrated with Cu/Ti and the carbon was subsequently burned out. The density and/or pore size still need to be decreased for potential ICF application.

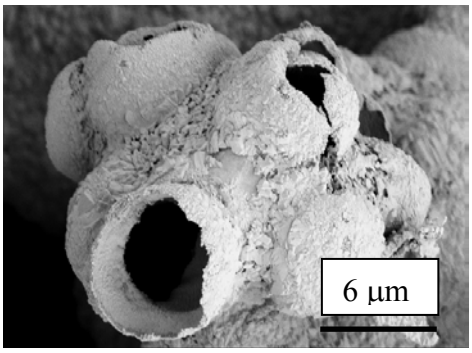

Figure 5. Scanning electron microscope image of porous Cu/Ti at 15% full density formed by templating with carbon spheres. The 6 μm fiducial is shown. Image courtesy of Joe Satcher (LLNL).

A new class of monolithic, transition metal oxide aerogels have been developed for use in ICF experiments. The approach is straightforward, inexpensive, versatile, and it produces monolithic microporous materials with high surface areas [Gash 2001]. In this technique epoxides are used as gelation agents for the sol-gel synthesis of transition metal aerogels from simple trivalent transition metal inorganic salts. The results show that rigid monolithic metal oxide aerogels can be prepared from solutions of their respective metal ion salts (Fe3+, Al3+, In3+, Ga3+, Zr4+ Hf4+, Ta5+, Nb5+, and W6+), provided the formal oxidation state of the metal ion is $\geq +3$. Conversely, when di-valent transition metal salts are used precipitated solids are the products. These transition metal aerogels can be used in double-shell ICF targets to help control the hydrodynamic instabilities.

X-ray backlighting for *in situ*, dynamic, radiographic imaging of ICF targets is a staple of ICF diagnostics. The radiographic images at useful resolution are almost always photon starved and generating multi keV photons for sufficient contrast has required development. Historically, solid targets, usually massive disks, have demonstrated efficiencies of only fractions of a percent for multi-keV photon energies. The efficiencies of these massive targets are compromised because much of the laser energy is deposited

in a (relatively) low-density region at the critical surface, while the region of the target dominating the radiation output may be a higher-density region that must be conductively heated. One hope to increase the efficiency of the solid targets is to heat volumetrically the whole target by using reduced solid density. Doped aerogels is a promising route. The doped aerogel material is formed by supercritical extraction of the solvent used to mix the dopant and silicon alkoxides. Fournier et al. [Fournier 2004] recently measured the production of $h\nu$ ~4.7 keV x-rays from low-density Ti-doped (3 At%) aerogel (ρ ~3 mg/cc) targets at the OMEGA laser facility, with the goal of maximizing x-ray output. The laser fully ionizes the target ($n(e)/n(crit) \leq 0.1$), and a laser-bleaching wave excites, supersonically, the high-Z emitter (Ti) ions in the sample. They found between 40 and 260 J of output with $4.67 \leq h\nu \leq 5.0$ keV.

4.0 Target Assembly

Many targets (ICF single shell, ICF double shell, Rayleigh-Taylor diagnostic targets) require complex assembly to tight tolerances [Hibbard 2004, Balkey 2004]. Assembly of the physics package may involve many micromachining and deposition steps and precision joining of parts with nanometer surface finish and micron features. Figure 6 shows the assembly of an ICF double shell. Generally the capsules must be positioned in the hohlraum with a formvar tent. The hohlraums frequently have diagnostic holes in them for mounting backlighters and other diagnostics. The hohlraum is mounted on a stalk usually with fiducials for laser alignment. Figure 7 is an optical micrograph of an assembled diagnostic target.

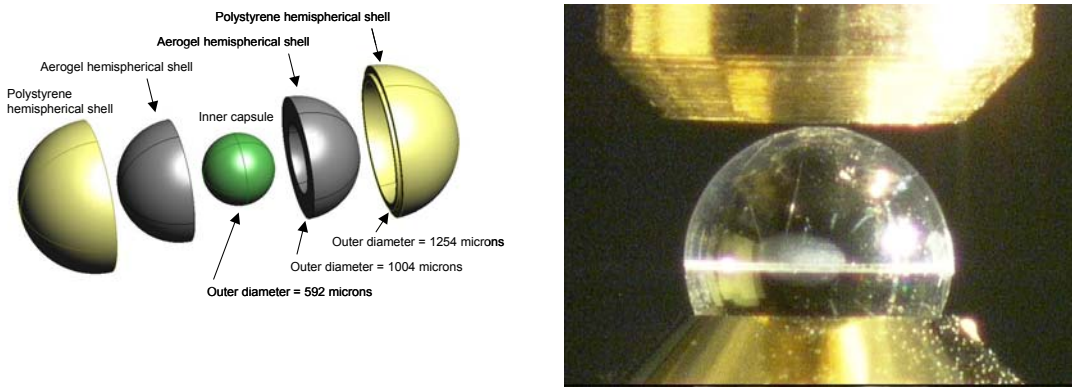

Figure 6. Exploded view of the double shell target (left) and a completed target in the vacuum chuck holder. Image courtesy of Robin Hibbard, LLNL.

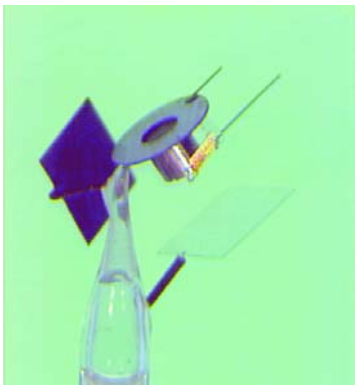

Figure 7. Optical microscope image of mounted target package showing backlighter positions and alignment fiducials. Image courtesy of Russ Wallace, LLNL.

Most ICF capsules require filling with either D_2 or DT gas. The standard method for filling is permeation filling at either room or elevated temperature. Capsules that have been produced by coating depolymerizable PAMS shells (e.g., CH shells) are too permeable to hold gas at room temperature. If the α-methyl styrene can diffuse out, the DT gas will also diffuse out rapidly. Poly (vinylalcohol) layers have been used to hold DT gas in the capsules. Aluminum coatings on CH shells can also be used to retain hydrogen gases. SiO_2 glass shells are retentive and can hold more than 60 atmospheres of DT gas with more than 2 week half-life (time for half the hydrogen gas to permeate in or out of the capsule). Permeation filling of high-Z metal inner shells is also possible. The permeation rate for hydrogen through Au/Cu at 500ºC is sufficient to fill a capsule to ~800 atmospheres in about one week [Shelby 1996]. Unfortunately, since the strength of the shell to hold such high pressures depends on the microstructure of the metal shell, heating the shell to 500ºC will likely lead to significant grain growth in the metal and weakening of the shell.

A second method for filling is the attachment of a fill tube to the capsule. The use of fill tubes has the advantage that the capsule can be filled and cryogenically cooled and the fuel assembled into a smooth shell after insertion into the target chamber. This technique does not require the extensive cryogenic infrastructure that a pre-filled and cryogenically assembled target would require. The fill tube is likely to be a silica capillary with 10 micron outer diameter and 6 micron inner diameter. The tube will have to be precision assembled in the 100-140 micron thick ablator and aligned with the 3-5 micron laser drilled hole in the ablator.

Non-uniformities in bond joints can cause asymmetries in the implosions. Ideally joints will introduce no change in material properties (density, opacity, sound velocity, and surface finish). In the recent double shell campaign at OMEGA, great care was taken to produce a robust bond joint between the hemispheres of the outer ablator shell [Hibbard 2004]. The bonding in this case was a two step process. The designed joint required the density of the adhesive match the density of the polystyrene shell to within 10 %. A step joint was designed so that the inner half of the step joint is mated and a 2micron gap is intentionally available for adhesive fill. The adhesive must wick into the 2 micron gap and completely fill it. Otherwise, voids in the joint would adversely affect performance.

The adhesive cannot have high-Z impurities or binders that degrade the ablator performance. Further, the adhesive should not wick past the inner step in the joint and into the nanoporous foam (carbonized resorcinol formaldehyde). The additional full density material would also degrade performance. Cyanoacrylate is applied around the perimeter of the joint by placing a droplet on the end of a camel hair. In the second step epoxy is applied to stabilize the joint during final machining of the outer surface. The epoxy is fully machined away during this machining step. By bonding prior to final machining of the outer ablator surface, precision dispensing of adhesive and crazing of the ablator surface is avoided.

In order to prevent asymmetric shell collision in double shell ICF targets the two shells must be concentric to within 5 microns. Figure 6 shows the components that are assembled to produce the concentric shells. Great care in the assembly is required. The precision machining produces dimensional errors of < 0.3 microns. Since three machined surfaces define the concentricity, concentricity within a micron is possible. However, the fragile nature of the carbonized resorcinol formaldehyde foam introduces the additional difficulty in meeting the 5 micron concentricity requirement. Minimal force during assembly is required so that the foam will not be crushed or deformed. Hence mechanical strength of the foam is an important consideration.

5.0 Target Characterization

A complete ICF experiment requires design, target fabrication and materials performance, and diagnostics. Target fabrication is not complete until the target specifications are characterized and metrologized in the “as built” configuration. Non-destructive evaluation of the assembled target requires “seeing” inside the target. Three probes have been applied to seeing inside the targets: x-rays, protons, and acoustic waves.

X-ray imaging of target assemblies is the most advanced of the characterization technologies and can provide many of the characterization analyses that are required.

Contact radiography involves placing the object to be characterized on the x-ray photographic film and illuminating the object with x-rays. The resolution is determined by the resolution of the film, typically about 1 micron. Figure 8 shows two orthogonal contact radiographs of ICF double shell targets. The integrity of the bond joint and the concentricity of the target can be measured. Resolution is insufficient to determine surface finish and metrology of the surface must be performed pre-assembly (see below).

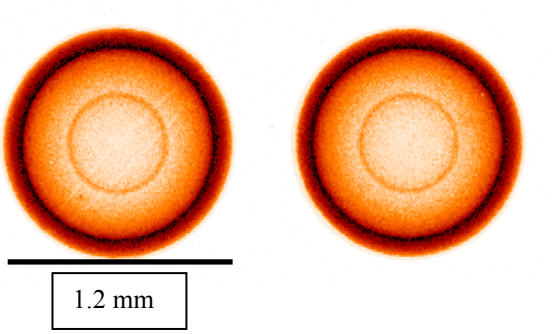

Figure 8. Contact radiograph of a double shell target. The bond joint is visible in the side view on the left. Top view is shown on the left. Resolution of the image is ~ 1micron. Image courtesy of Russell Wallace, LLNL

The key strength of x-ray full-field microscopy is the large penetration depth of x-rays into matter, which allows one to image the interior of opaque objects. Combined with tomographic techniques, the three-dimensional inner structure of an object can be reconstructed without the need for difficult and destructive sample preparation [Schroer 2004]. Point projection x-ray microscopes are currently commercially available. These microscopes can typically perform tomographic imaging and reconstruction of an object. Resolution and field of view change together in these microscopes. Typically a ~2 micron resolution with 0.5 - 1 millimeter field of view can be achieved. Higher resolution (0.5micron) can be achieved with smaller fields of view. Figure 9 shows a point projection image of a portion of a mock double-shell target.

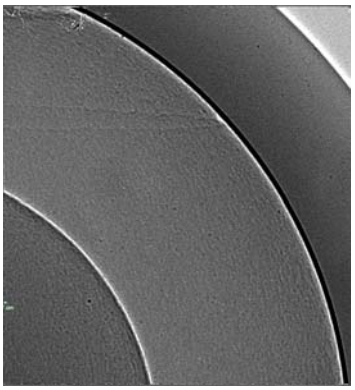

Figure 9. Phase and amplitude contrast image of a mock double shell target taken with ~5 keV x-rays from a point projection microscope. Image courtesy of Wenbing Yun, Xradia, Concord, CA.

X-ray projection microscopy which utilizes phase contrast to enhance the quality and information content of images has been developed [Mayo 2003]. By combining fine x-ray source with an appropriate imaging geometry, phase contrast arising from Fresnel diffraction at edges and boundaries within the sample leads to images with greatly enhanced edge detail. Phase-retrieval algorithms have been developed for quantitative determination of the projected phase shift in the object-plane from either a single image or multiple images acquired at different energies or magnifications. Figure 9 shows a fine defect intentionally machined into the 50 mg/cm3 carbonized resorcinol

formaldehyde foam. Because of the low-density and low-Z of the foam, amplitude contrast alone would be insufficient to detect this flaw. However, combining phase contrast and amplitude contrast made this few micron flaw in the foam discernible. This technique is also capable of imaging DT ice structure inside optically opaque ablators (Be).

Structural properties of nanoporous materials can be studied by small-angle X-ray scattering [Pahl 1991]. The measured SAXS profiles reveal a scattering power depending upon synthetic conditions of the nanoporous material. Structural features such as pore distribution from 2-100 nm can be determined from the scattering data. Radii of gyration R(g) are computed and appear to be a measure of the pore (cell) size. Since scattering can be from localized columns (sub micron diameters) of material, density gradients and spatial inhomogeneity of the pores can be measured.

The complementary techniques of ion microtomography (IMT) and particle-induced x-ray emission (PIXE) are used to provide submicron-scale characterization of inertial confinement fusion (ICF) targets for density uniformity, sphericity, and trace-element spatial distributions [Antolak 1992]. 1% total electron density determinations using IMT with spatial resolution approaching 2 μm can be obtained. Utilizing PIXE, dopant and impurity distributions with elemental detection sensitivities on the order of a few parts per million can be determined.

One potentially valuable method for evaluating the quality of ICF targets is resonant ultrasound spectroscopy (RUS). When applied to simple geometries, such as layered spheres or rectangular parallelepipeds, RUS may yield significant information about alloy homogeneity, elastic constants, cavity geometry, the presence of gross defects such as cracking or hemishell bonding problems, and properties of interior fluids. The strengths of RUS techniques for ICF target characterization include applicability at all temperatures of interest with a single apparatus, high sensitivity in frequency spectral measurements, and the inherent acoustic indifference to optically opaque samples. The acoustic cavity resonance structure can be used to calculate cavity boundary perturbation amplitudes [Asaki 1998]. Experiments have also been conducted in which the D_2 fill pressure has been determined for several closed millimeter-size aluminum and beryllium shells [Asaki 1999]. The vibrational resonance frequency spectrum of the shells was used to calculate the sound velocity of the interior gas. This velocity, along with the equation-of-state, determined the gas pressure and density. The accuracy in determining the fill conditions is within 0.5% in both pressure and density for near critical density ($\rho \geq 9$ mol/L) gas.

Measuring the surface perturbation of capsules is of considerable importance. Two techniques are available for metrology of the shell surface: interferometry and atomic force profiling.

White light interferometry is used to determine thickness and uniformity of transparent shells [Weinstein 1982]. Laser (holographic) interferometry is used to measure cryogenic

layer uniformity [Bernat 1982]. Commercial instruments for capsule measurements are available.

A profilometer based on an atomic force microscope combined with a precision rotary air bearing has been developed [McEachern 1995]. In this instrument the shell is placed in vacuum chuck and rotated with the precision rotatary air bearing. The AFM tip on its piezo-electric mount profiles the surface to within 1 nm with cantilever deflection (force feedback – contact mode). With reorientations of the shell, a power spectrum (the square of the mode amplitude as a function mode number) for legendre modes (the ratio of the capsule circumference to the wavelength of the perturbation) from 2 to 10,000 for the entire sphere can be calculated. The measured/calculated power spectrum is used as input in implosion simulations.

Acknowledgements

Work was performed under the auspices of the U.S. Department of Energy by Lawrence Livermore National Laboratory under Contract No. W-7405-ENG-48. AVH thanks Dr. Peter Amendt for a critical reading and suggested improvements in this article.

6.0 References

[Alexander2004] Alexander A. J., Cooley, J. C., Thoma, D. J., and Nobile, A., "Production of fine grained Berylium-6Wt.% Cu for Fusion Ignition Capsules by Arc Melting and Equal Channel Angular Extrusion," Fusion Sci. Technol. **45**, 137 (2004).

[Amendt 2002] Amendt, P., Colvin, J. D., Tipton, R. E., Hinkel, D. E., Edwards, M. J., Landen, O. L., Ramshaw, J. D., Suter L. J., Varnum W. S. and Watt, R. G., " Indirect-Drivce Noncryogenic Ignition targets for the National Ignition Facility: Design and Analysis," Phys. Plasmas **9**, 2221 (2002).

[Amendt 2003] Amendt, P., Colvin, J. D., Ramshaw, J. D., Robey, H. F., and Landen, O. L., "Modified Bell–Plesset Effect with Compressibility:Application to Double-Shell Ignition Target Designs**,"** Phys. Plasmas **10**, 820 (2003)

[Amendt 2004] Amendt, P., Robey, H. F., *et al.,* Submitted to PRL

[Antolak 1992] Antolak AJ, Pontau AE, Morse DH, Weirup DL, Heikkinen DW, Cholewa M, Bench GS, Legge GJF, "Ion Microtomography and Particle-Induced X-Ray-Emission Analysis of Direct Drive Inertial Confinement Fusion-Targets," Journal Of Vacuum Science & Technology A-Vacuum Surfaces And Films **10**, 1164-1169 (1992)

[Asaki 1998] Asaki TJ, Hoffer JK, Sheliak JD, "Ultrasonic characterization of inertial confinement fusion targets," Fusion Technol **33**, 171-181 (1998)

[Asaki 1999] Asaki TJ, "Ultrasonically determined fill pressure and density in closed spherical shells," Fusion Technology **35**, 126-130 (1999)

[Balkey 2004] Balkey, M. M., Day, R. D., Batha, S. H., Elliot, N. E., Pierce, T., Sandoval, D. L., Garrard, K. P., and Sohn, A., "Production and Metrology of Cylindrical Inertial Confinement Fusion Targets with Sinusoidal Perturbations," Fusion Sci. Technol. **45**, 107 (2004).

[Baumann 2003] Baumann TF, Satcher JH, "Homogeneous incorporation of metal nanoparticles into ordered macroporous carbons," Chemistry of Materials **15**, 3745-3747 (2003).

[Bernat 1982] Bernat, T. P., Darling, D. H., Sanchez, J. J., "Applications of Holographic Interferometry to Cryogenic ICF target characterization," J. Vac. Sci. Technol. **20**, 1362 (1982).

[Bourdinaud 1976] Bourdinaud M, Cheze JB, Thevenin JC, "Use of Silica Aerogel for Cherenkov Radiation Counter," Nucl Instrum Methods **136**, 99-103 (1976).

[Collins] Collins, G. W., Bernat, T. P., Mapoles, E. R., Duriez, C., "Heat flux induced changes to multicrystalline D_2 surfaces," LLNL Report No. UCRL-JC-124261.

[Erlebacher 2001] Erlebacher, J., Aziz, M. J., Karma, A., Dimitrov, N., Sieradzki, K., "Evolution of Nanoporosity in Dealloying," Nature **410**, 450 (2001).

[Erlebacher 2003] Erlebacher, J., Sieradzki, K., "Pattern Formation during Dealloying," Scripta Materialia **49**, 991 (2003).

[Fournier 2004] Fournier KB, Constantin C, Poco J, Miller MC, Back CA, Suter LJ, Satcher J, Davis J, Grun J, "Efficient multi-keV x-ray sources from Ti-doped aerogel targets,**"** Physical Review Letters 92, Art. No. 165005 (2004)

[Gash 2001] Gash AE, Tillotson TM, Satcher JH, Hrubesh LW, Simpson RL, "New sol-gel synthetic route to transition and main-group metal oxide aerogels using inorganic salt precursors," Journal of Non-Crystalline Solids **285**, 22-28 (2001).

[Hibbard 2004] Hibbard, R. L., Bono, M. J., Amendt, P., Bennett, D. W., Castro, C., "Precision Manufacturing of Inertial Confinement Fusion Double Shell Laser Targets for OMEGA," Fusion Sci. Technol. **45**, 117 (2004).

[Hoppe 2002] Hoppe, M. L., "Recent developments in making glass shells from silicon doped GDP shells" Fusion Science and Technology **41**, 234-237 (2002).

[Jankowski 2002] Jankowki, A. F., Wall, M. A., van Buuren, A. W., Nieh, T. G., Wadsworth, J., "From Nanocrystalline to Amorphous Structure in Beryllium-Based Coatings," Acta Materialia **50**, 4791 (2002).

[Letts 2004] Letts, S. A., Anthamatten, M., Buckley, S. R., Fearon, E., Nissen, A. E. H., and Cook, R. C. "Progress Toward Meeting NIF Specifications for Vapor Deposited Polyimide Ablator Coatings," Fusion Sci. Technol. **45**, 180 (2004).

[Lindl 1998] Lindl, J. D., *Inertial Confinement Fusion* (Springer-Verlag, New York, 1998)

[Lindl 2004] Lindl, J. D., Amendt, P., Berger, R. L., Glendinning, S. G., Glenzer, S. H., Haan, S. W., Kauffman, R. L., Landen, O. L., and Suter, L. J., „The Physics basis for ignition using indirect drive targets on NIF," Phys. Plasmas **11**, 339 (2004).

[Lindl 1983] Lindl, J. D., "Hydrodynamic and Plasma Stability Limitations on the Choice of Laser Wavelength for Radiation Driven ICF Implosions," Laser Program Annual Report (1983), Lawrence Livermore National Laboratory, Livermore, CA, UCRL-50055-83, pp. 2-40 to 2-46 (unpublished).

[Mayo 2003] Mayo SC, Miller PR, Wilkins SW, Davis TJ, Gao D, Gureyev TE, Paganin D, Parry DJ, Pogany A, Stevenson AW, **"**Applications of phase-contrast X-ray microscopy in an SEM," Journal de Physique IV **104**, 543-546 (2003).

[McEachern 1995] McEachern, R. L., Moore, C. E., Wallace, R. J., "Design, Performance, and Application of an Atomic Force Microscope-Based Profilometer," J. Vac. Sci. Technol. A **13**, 983 (1995).

[Mehlhorn 2003] Mehlhorn TA, Bailey JE, Bennett G, Chandler GA, Cooper G, Cuneo ME, Golovkin I, Hanson DL, Leeper RJ, MacFarlane JJ, Mancini RC, Matzen MK, Nash TJ, Olson CL, Porter JL, Ruiz CL, Schroen DG, Slutz SA, Varnum W, Vesey RA, "Recent experimental results on ICF target implosions by Z-pinch radiation sources and their relevance to ICF ignition studies," Plasma Physics and Controlled Fusion **45**, A325-A334 Suppl. 12A (2003).

[Nobile 2004] Nobile, A. Dropinski, S. C., Edwards, J. M., Rivera, G., Margevicius, R. W., Sebring, R. J., Olson, R. E., and Tanner, D. L., "Fabrication and Characterization of Targets for Shock Propogation and Radiation Burnthrough Measurements on Be 0.9 At. % Cu Alloy," Fusion Sci. Technol. **45**, 127 (2004).

[Orzechowski 1996] Orzechowski, T. J., Rosen, M. D., Kornbulm, H. N., Porter, J. L., Suter, L. J., Thiessen, A. R. , and Wallace, R. J., "The Rossland Mean Opacity of a Mixture of Gold and Gadolinium at High Temperature," Phys. Rev. Lett. 77, 3545 (1996).

[Pahl 1991] Pahl R, Bonse U, Pekala Rw, Kinney Jh, "SAXS Investigations on Organic Aerogels," Journal of Applied Crystallography 24, 771-776 (1991).

[Pekala 1989] Pekala, R. W., "Organic Aerogels from the Polycondensation of Resorcinol with Formaldehyde,**"** J. Mater. Sci. **24**, 3221 (1989)

[Pierre 2002] Pierre, A. C., Pajonk, G. M., "Chemistry of aerogels and their applications," Chem Rev 102, 4243 (2002).

[Pugh 2003] Pugh, D. V., Dursun, A., and Corcoran, S. G., "Formation of Nanoporous Platinum by Selective Dissolution of Cu from $Cu_{0.75}Pt_{0.25}$," J. Mater. Res. 18, 216 (2003).

[Rosen 2004] Rosen, M. D. and Hammer, J. " ", Submitted to Phys Rev Lett.

[Schroer 2004] Schroer CG, Cloetens P, Rivers M, Snigirev A, Takeuchi A, Yun WB, "High-resolution 3D imaging microscopy using hard x-rays," MRS Bulletin **29**, 157-165 (2004).

[Shelby 1996] Shelby, J. E., *Handbook of Gas diffusion in Solids and Melts*, (ASM International, Materials Park, OH, 1996).

[Sieradzki 1992] Li, R., and Sieradzki, K., "Ductile-Brittle Transition in Random Porous Au," Phys. Rev. Lett. **68**, 1168 (1992).

[van Swygenhoven 2004] Budrovic Z, Van Swygenhoven H, Derlet PM, Van Petegem S, Schmitt B, "Plastic deformation with reversible peak broadening in nanocrystalline nickel," Science **304**, 273-276 (2004).

[van Swygenhoven 2003] van Swygenhoven H, Derlet PM, Budrovic Z, Hasnaoui A, "Unconventional deformation mechanism in nanocrystalline metals?" Zeitschrift Fur Metallkunde **94**, 1106-1110 (2003).

[Varnum] Varnum W. S., Private Communication.

[Velev 1999] Velev OD, Tessier PM, Lenhoff AM, Kaler EW, "Materials - A class of porous metallic nanostructures," Nature **401**, 548-548 (1999).
[Weinstein 1982] Weinstein, B. W., "Physical Measurements of Inertial Confinement Fusion Targets," J. Vac. Sci. Technol. **20**, 1349 (1982).
[Wolf 2004] Yamakov V, Wolf D, Phillpot SR, Mukherjee AK, Gleiter H, "Deformation-Mechanism Map for Nanocrystalline Metals by Molecular-Dynamics Simulation," Nature Materials **3**, 43-47 (2004).